Masuda *et al.*
Progress in Earth and Planetary Science (2022) 9:65
https://doi.org/10.1186/s40645-022-00527-x

Progress in Earth and Planetary Science

RESEARCH ARTICLE

Open Access

To what extent tsunami source information can be extracted from tsunami deposits? Implications from the 2011 Tohoku-oki tsunami deposits and sediment transport simulations

Hidetoshi Masuda[1*], Daisuke Sugawara[2], Tomoya Abe[3] and Kazuhisa Goto[4]

Abstract

A quantitative understanding of paleotsunamis is a significant issue in tsunami sedimentology. Onshore tsunami deposits, which are geological records of tsunami inundation, are used to reconstruct paleotsunami events. Numerical models of tsunami hydrodynamics and tsunami-induced sediment transport are utilized in such reconstructions to connect tsunami deposit characteristics, flow conditions, and (paleo-) tsunami sources. Recent progress in tsunami numerical modeling has increased the possibility of developing a methodology to estimate paleotsunami sources from tsunami deposits. Several previous studies have estimated paleotsunami sources using tsunami sediment transport simulations. However, the accuracy of paleotsunami source estimation has not yet been explored. Thus, to bridge this research gap, in this study, we showed the potential and limitations of deposit-based tsunami source estimation based on the 2011 Tohoku-oki tsunami deposit data on the southernmost part of the Sendai Plain, northeastern Japan. The tsunamigenic megathrust along the Japan Trench was divided into ten subfaults having similar lengths and widths. The hypothetical source models with varying slips on each subfault were examined by comparing the depositional volume and sediment source of onshore tsunami deposits. Due to limited information on the depositional area of the tsunami deposits used in the modeling, slips only in some parts of the entire tsunami source region could be estimated. The fault slip was slightly overestimated but could be compared with previous well-constrained source models. Thus, these results indicated that vast high-quality datasets of tsunami deposits can improve the accuracy of paleotsunami source estimation. It is also suggested that the amplitude of the receding wave affects the erosion pattern from the shoreface to the nearshore area. Although sufficient data for paleotsunami source estimation are lacking, an effective combination of tsunami deposit data and sediment transport simulations potentially improves the accuracy of the source estimation. The results will contribute to developing a framework of deposit-based paleotsunami source modeling and assessing its accuracy.

Keywords: 2011 Tohoku-oki tsunami, Tsunami deposit, Paleotsunami, Tsunami source estimation, Tsunami sediment transport simulation

1 Introduction

A tsunami source is defined as a region in which the water level is displaced from the still water level. In the case of tsunamigenic earthquakes, tsunami sources are often described by static focal parameters that determine coseismic crustal deformation. Source modeling of modern tsunamis using instrumental observational data is a

*Correspondence: hidetoshi.masuda.s3@dc.tohoku.ac.jp

[1] Department of Earth Science, Graduate School of Science, Tohoku University, 6-3 Aramaki Aza-Aoba, Aoba-ku, Sendai, Miyagi 980-8578, Japan
Full list of author information is available at the end of the article

major approach to understanding the focal region, size, and rupture process of such tsunamigenic earthquakes. Conversely, source modeling of earlier (or paleo-) tsunamis, such as those that occurred hundreds to thousands of years ago, is crucial for the long-term assessment of tsunamigenic earthquakes.

Source modeling of modern and paleotsunamis employs different approaches due to differences in the available data. Inverse modeling of instrumental records, such as oceanographic (tsunami), seismic, and geodetic data, is commonly used to determine the focal parameters of modern tsunamigenic earthquakes (Satake 1987; Satake et al. 2013; Iinuma et al. 2012; Yamazaki et al. 2018). Contrastingly, paleotsunami source modeling utilizes historical records (e.g., documented run-up heights) and geological records (e.g., tsunami deposits), which rarely provide sufficient quantitative information for inverse modeling as conducted for modern events.

Tsunami deposits provide geological information on the inundation extents, flow conditions, and repeating run-up and backwash flows (Fujiwara 2008). They have widely been used for source modeling of paleotsunamis (Satake et al. 2008; Namegaya and Satake 2014; Butler et al. 2014; Ioki and Tanioka 2016; Sugawara et al. 2019; Dourado et al. 2021). Sandy tsunami deposits have been extensively studied because they can be easily identified as high-energy depositional events in stable environments, such as coastal lowlands (Minoura and Nakaya 1991). Deposit-based tsunami source modeling typically employs a trial-and-error approach (Aida 1977), which exhaustively examines hypothetical source models using forward tsunami simulation to assess which model best explains the distribution of known tsunami deposits.

Most conventional reconstructions of deposit-based paleotsunami sources have utilized only tsunami deposit distribution as a constraint of minimum inundation caused by tsunamis. These reconstructions compare the observed characteristics of tsunami deposits with the hydrodynamic simulations of tsunamis. However, recent post-tsunami field surveys (Srinivasalu et al. 2007; Goto et al. 2011; Abe et al. 2012) have reported significant gaps between the tsunami inundation limits and the maximum inland extent of sandy tsunami deposits; furthermore, these gaps enlarge with increasing inundation distance (Abe et al. 2012). Thus, this increased concerns for the application of hydrodynamic simulations in deposit-based tsunami source estimation because the gap between tsunami inundation and deposit extent can result in possible underestimation of the tsunami size. In the meanwhile, information associated with tsunami deposits, such as thickness, volume, grain size, and sediment source, was not fully included in deposit-based paleotsunami source modeling.

Numerical modeling of tsunami-induced sediment transport has recently been applied in paleotsunami studies (Sugawara et al. 2014a; Sugawara 2021). Along with hydraulic data, information on deposit thickness and erosion depth can be obtained from tsunami sediment transport simulations and the results of the simulations can be compared directly with the sedimentary data of tsunami deposits. As the application of tsunami sediment transport simulations in tsunami deposit research is still at its nascent stage, examples of paleotsunami source modeling using sediment transport simulations are scarce (Sugawara et al. 2019; Dourado et al. 2021; Nakanishi and Ashi 2022). Thus, the validity and limitations of the application of tsunami sediment transport simulations in tsunami source modeling have not yet been explored.

The possibility of tsunami source estimation using sediment transport simulations on the 2011 Tohoku-oki tsunami has been previously explored (Gusman et al. 2018; Hisamatsu et al. 2019). Gusman et al. (2018) conducted a sensitivity analysis with varying tsunami amplitudes and periods and found that the simulated deposit thickness and grain-size distribution were controlled by tsunami characteristics, such as wave amplitude and period. However, the relationship between the simulated deposit distribution and tsunami source parameter was not directly analyzed. Hisamatsu et al. (2019) estimated the source parameter of the 2011 Tohoku-oki tsunami by utilizing tsunami sediment transport simulations and tsunami deposit data. Additionally, they used the conical fault model proposed by Hisamatsu et al. (2017) and tsunami deposit data from three different sites on the Pacific coast of Tohoku. Their deposit-based source modeling well reproduced the moment magnitude of the earthquake; however, the maximum slip was underestimated. Nevertheless, rectangular fault models are still dominantly used in source estimation of both modern and paleotsunamis (Satake et al. 2013; Yamazaki et al. 2018; Sugawara et al. 2019; Dourado et al. 2021; Nakanishi and Ashi 2022). Thus, an examination of the framework using the rectangular fault model can be useful to compare the results with those of the rectangular model reported in previous studies.

This study aimed to estimate tsunami sources based on the 2011 Tohoku-oki tsunami deposit data from a small area of ~ 0.8 km^2 on the southernmost part of the Sendai Plain. To acquire suggestions for paleotsunami source estimation, we initiated the source modeling from the standpoint that has not been revealed regarding the slip distribution and paleotsunami research, even though vast knowledge on the earthquake has been accumulated in the last decade. We explored the tsunami source based on the numerical simulation of sediment transport that occurred due to the tsunami.

High-density tsunami deposit data acquired from the southernmost part of the Sendai Plain (Abe et al. 2020) along with pre- and post-tsunami topographic data were used for benchmark and model inputs. Further, the slip distribution of the estimated tsunami source was discussed by comparing it with the results of other tsunami source models reported in previous studies.

2 Study area and sedimentary data

Deposits of tsunamis in the Sendai Plain, such as the 869 Jogan, 1454 Kyotoku, 1611 Keicho, and 2011 Tohoku-oki, have been previously examined in detail (Sawai et al. 2008, 2012, 2015; Abe et al. 2012, 2020; Shinozaki et al. 2015). The 2011 Tohoku-oki tsunami caused extensive inundation throughout the Sendai Plain (Mori et al. 2012; Haraguchi and Iwamatsu 2013). The present study examined the 2011 Tohoku-oki tsunami and its deposits on the southernmost part of the Sendai Plain in Yamamoto town, Miyagi Prefecture, northeastern Japan (Fig. 1). In the study area, tsunami inundation reached 3 km from the coastline, with a maximum flow depth of 10 m (Suppasri et al. 2012).

Before the 2011 Tohoku-oki tsunami, a sandy beach (width of 0–80 m) was developed along the coastline. The beach ridge (elevation of 2–3 m from Tokyo Peil [TP]) behind the sandy beach was covered by a coastal forest, which was devastated by the 2011 Tohoku-oki tsunami. Subsequently, a coastal dike (6.2 m from TP) was built between the beach ridge and the backshore (Abe et al. 2020). The elevation of the lowland, which is used mainly for rice paddies, is 2–3 m. The drowned valley and the surrounding Pliocene sandstone hills (30 m from TP) are developed in the west of the lowland (Fujita et al. 1988). A small coastal pond, Suijin-numa, partially covers the entrance of the drowned valley.

Sedimentary features, such as thickness, grain size, and sedimentary structures, of sandy and muddy tsunami deposits were collected from 172 sites in the drowned valley and the Suijin-numa pond to examine their spatial distribution and sediment source and budget (Abe et al. 2020; Fig. 1c). The tsunami deposits on the study area, as reported by Abe et al. (2020), are summarized as follows: The maximum thickness of the sandy tsunami deposit was 40 cm at ~270 m inland from the coastline. These deposits showed landward thinning and fining trends. In addition, the sandy deposits near the coastline and on the bottom of the Suijin-numa pond comprised one to four subunits associated with repeating run-up and backwash flows. Based on the eroded area and the grain-size distribution, the main sources of the sandy tsunami deposits were estimated as sandy beach and dunes.

3 Methods

3.1 Numerical model and inputs

A two-dimensional horizontal (2DH) tsunami sediment transport model (TUNAMI-STM; Sugawara et al. 2014b; Yamashita et al. 2016) was employed in this study. In this model, a depth-averaged tsunami hydrodynamic model, TUNAMI-N2 (Goto et al. 1997), which is based on the nonlinear long wave theory, was coupled with the sediment transport model (STM) proposed by Takahashi et al. (2000). The STM considers sediment exchange between the bed and suspended loads assuming a single grain-size class of the sediments. Previous studies have extensively utilized TUNAMI-STM and its derivatives to investigate tsunami-induced sediment transport due to the 2011 Tohoku-oki earthquake (Sugawara et al. 2014b; Yamashita et al. 2016, 2018; Arimitsu et al. 2017; Kusumoto et al. 2020) and to model the paleotsunami source of the 1867 Keelung earthquake (Sugawara et al. 2019). Sugawara et al. (2014b) demonstrated that the general trend of deposit thickness along orthogonal transects to the shoreline can be reproduced using STM. Yamashita et al. (2016) showed that the simulated sediment volumes of erosion and deposition caused by the Tohoku-oki tsunami in Hirota Bay on the Sanriku Coast were roughly consistent with observed volumes. The model has been comprehensively described by Sugawara et al. (2014b) and Yamashita et al. (2016).

A nesting grid system was used to optimize the computational efficiency and resolution of numerical modeling. The computational domain was divided into six-layered domains (R1–R6), with varying spatial resolutions and extents. Domain R1 has a spatial resolution of 1215 m and covers the entire interplate tsunami source region along the Japan Trench, whereas Domains R2–R6 have spatial resolutions ranging from 405 to 5 m with a constant ratio of 1/3. TUNAMI-N2 simulated tsunami propagation and inundation in all domains, while sediment transport simulations were performed only in Domain R6 (Fig. 1a). The numerical analyses were conducted for 3 h after the earthquake occurred. A temporal resolution of 0.1 s was selected to maintain numerical stability (i.e., Courant–Friedrichs–Lewy condition).

Bathymetric data were acquired from the public dataset provided by the Central Disaster Management Council, Cabinet Office, Government of Japan (http://www.bousai.go.jp/kaigirep/chuobou/senmon/nihonkaiko_chisimajishin/index.html) and the M7005 bathymetric chart published by the Japan Hydrographic Association. Topography data, which were based on the 5-m mesh digital elevation model (DEM) acquired using the light detection and ranging (LiDAR) technique, were provided by the Geospatial Authority of Japan (https://www.gsi.go.jp/kiban/). Both datasets were collected before the 2011

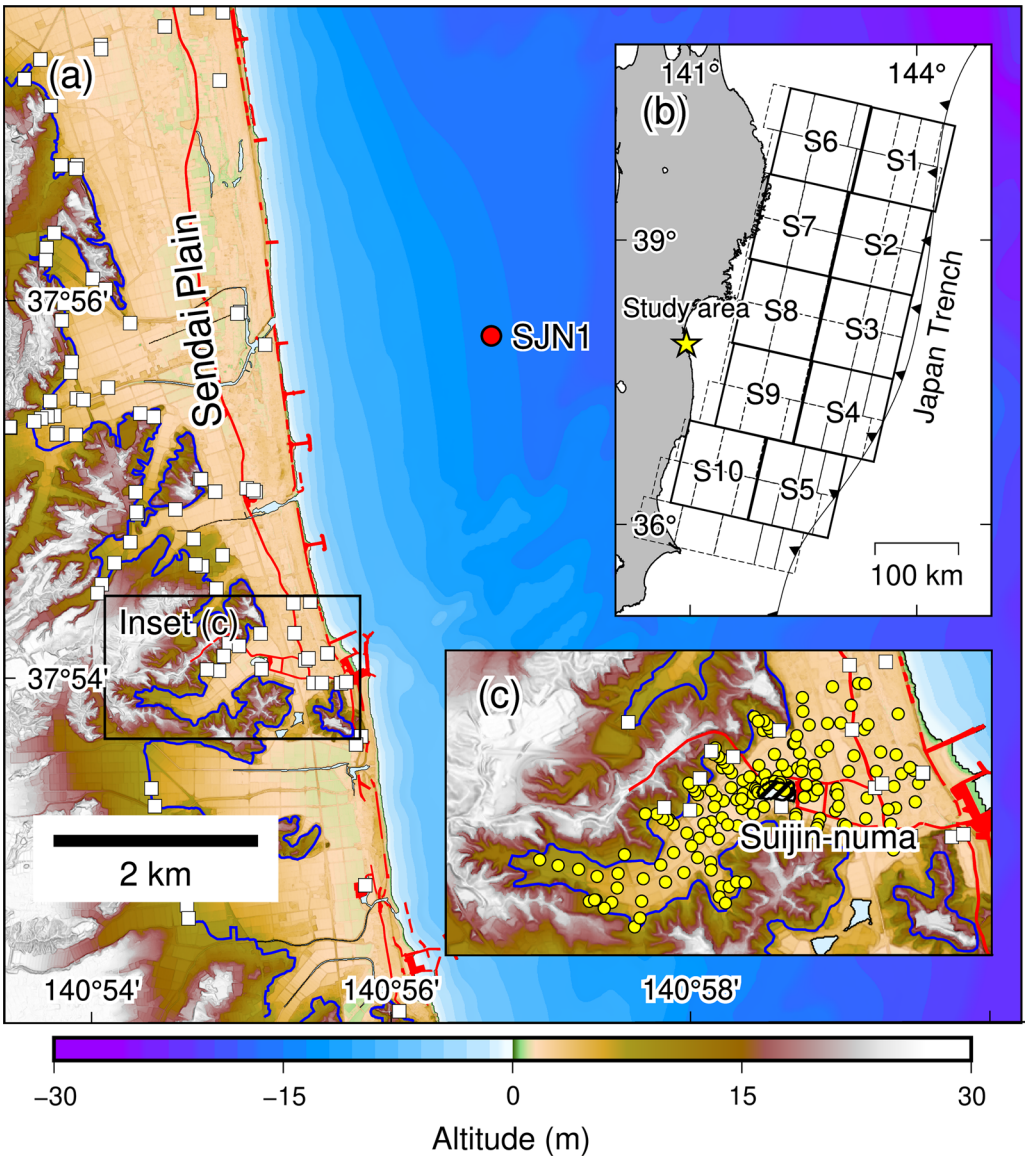

Fig. 1 Study area and fault models. **a** Topography and bathymetry map of the calculated Domain R6. White rectangles and red polygons indicate the survey point of tsunami trace height (Mori et al. 2012) and fixed bed, respectively. The blue line represents the inundation limit (Haraguchi and Iwamatsu 2013). **b** Fault models. Bold solid and thin dashed rectangles indicate the geometry of the fault model proposed by Hayashi and Koshimura (2012) and Satake et al. (2013), respectively. **c** Enlarged view around the Suijin-numa pond. Yellow circles represent the survey points of tsunami deposits (Abe et al. 2020)

Tohoku-oki earthquake, and a Cartesian coordinate system based on the transverse Mercator Projection (Japan Geodetic Datum 2000, Zone 10) was used.

Manning's roughness coefficient (0.025 $s/m^{1/3}$), which represents the friction on bare ground and the ocean floor (Kotani et al. 1998; Sugawara et al. 2014b), was assumed in all computational domains to evaluate bottom friction in the modeling of tsunami propagation and inundation. The initial tide level was set at − 0.5 m based on the tidal level at the Soma Port, which is located ~7 km south of the study area, when the earthquake occurred. Part of the engineered headlands, coastal dikes, and roads that were not damaged by the 2011 tsunami were assumed non-erodible in the tsunami sediment transport simulations (Sugawara et al. 2014b).

According to the results of the grain-size analysis described by Abe et al. (2020), the average median grain size of the tsunami deposits is ~1.9 ϕ (i.e., ~0.268 mm).

Thus, in the simulations conducted in the present study, we assumed the single grain size as 0.267 mm, which has been used in the flume experiment by Takahashi et al. (2011). The settling velocity of sand in still water was firstly calculated by Rubey's (1933) formula and then dynamically corrected considering hindered settling in the concentrated suspended sediments (Richardson and Zaki 1954; van Rijn 2007). Critical friction velocity, which is a function of grain size, was evaluated according to Iwagaki (1956). Grain-size-dependent parameters α and β, for bedload and exchange rates, determined by Takahashi et al. (2011) were used. Manning's roughness coefficient for STM is independent of that for TUNAMI-N2 (Yamashita et al. 2016). As the Manning's roughness coefficient for sand beds is difficult to constrain empirically, a value of 0.015 s/m$^{1/3}$ for STM was employed to calculate the friction velocity for the sediment transport simulations by optimizing the resulting deposition of the reference simulation (see Sects. 3.2.2 and 4.1).

3.2 Procedures

3.2.1 Metrics for comparing simulations and observations

Although STM can reproduce the overall trend of deposit thickness, the simulated deposit thickness at a given point is generally scattered around the observed value (Sugawara et al. 2014b, 2015). This can be associated with local variations in deposit thickness due to the effects of microtopographies on tsunami flow and sediment transport process (Hori et al. 2007; Fujiwara and Tanigawa 2014). The sparsely observed data cannot resolve the local variability of the deposit thickness comprehensively, while the simulated deposit thickness exhaustively covers all computational grids. Thus, simulations can reproduce the details of the local variability in the deposit thickness if the spatial grid size and precision of the topographic data are sufficiently high to resolve the microtopographies. In the present study, we adopted the LiDAR-based DEM with a spatial grid spacing of 5 m to numerically express such microtopographies. To avoid direct comparison at the scattered data points, we used observed and simulated deposit volumes in the study area based on the approach employed by Dourado et al. (2021), who compared the core-based depositional volume and calculated volume in several scenarios to select the most suitable source model for the 1755 Lisbon tsunami. The depositional volume was precisely estimated using sufficient sedimentary data and was potentially available as a constraint of deposit-based source modeling.

The thickness data of 162 points from 174 samples obtained by Abe et al. (2020) were used to estimate the observed deposit volume. In this study, we used the thickness of the sandy tsunami deposits because the STM cannot analyze muddy sediment transport.

Gridded data of the observed deposit thickness in the study area (Fig. 2b) were generated using the adjustable tension continuous curvature spline interpolation (surface module in the Generic Mapping Tools version 6; Smith and Wessel 1990; Wessel et al. 2019). The gridded thickness data (>0 m) were then used to calculate the deposit volume after clipping data through a polygon, which included the inundation limit of the reference simulation (see Sects. 3.2.2 and 4.1) on the valley floor and coastward limit of the observed thickness data on the coastal plain. As a result, it is estimated that 85,336 m^3 of tsunami deposits was lying on 823,204 m^2 of the inundation area, based on the observed deposit thickness. This estimated deposition volume was used as a constraint of the source modeling. To reduce the difference in spatial density of the observed and simulated data and for better comparison, simulated deposit thicknesses extracted from the survey points of Abe et al. (2020) were interpolated in the same way as the observed data, considering the difference in the spatial characteristics of the observed and simulated data. Note that the inundation limits used for clipping varied in each scenario.

3.2.2 Model calibration

The 2011 Tohoku-oki tsunami was initially numerically simulated using a published source model to validate the simulation with the given parameter settings. The tsunami source model by Satake et al. (2013) that resolves the spatiotemporal evolution of the slip distribution was used to calculate seafloor deformation and the resulting initial tsunami waveform. Okada's (1985) formula was used to calculate the seafloor deformation considering the effect of horizontal motion of a sloping seafloor (Tanioka and Satake 1996).

The boundary condition (flux) between domains R4 and R5 was calibrated based on the geometric mean K and geometric standard deviation κ of the ratio of observed tsunami height to simulated height (Aida 1978), following Sugawara et al. (2014b). The tsunami trace height datasets reported by the 2011 Tohoku Earthquake Tsunami Joint Survey Group (Mori et al. 2012) within Domain R6 were employed regardless of the reliability index of each datum.

The preliminary tsunami hydrodynamic simulation and sediment transport simulation using the original source parameters given by Satake et al. (2013) underestimated the tsunami measurements in the study area. Aida's (1978) criteria for model validation, which assesses the ratio of observed tsunami heights to simulated heights, was found to be $K = 1.22$ for the geometric mean and $\kappa = 1.22$ for the geometric standard deviation for 59 trace heights within the computational Domain R6 (Additional file 1: Fig. S1). Moreover, the thicknesses

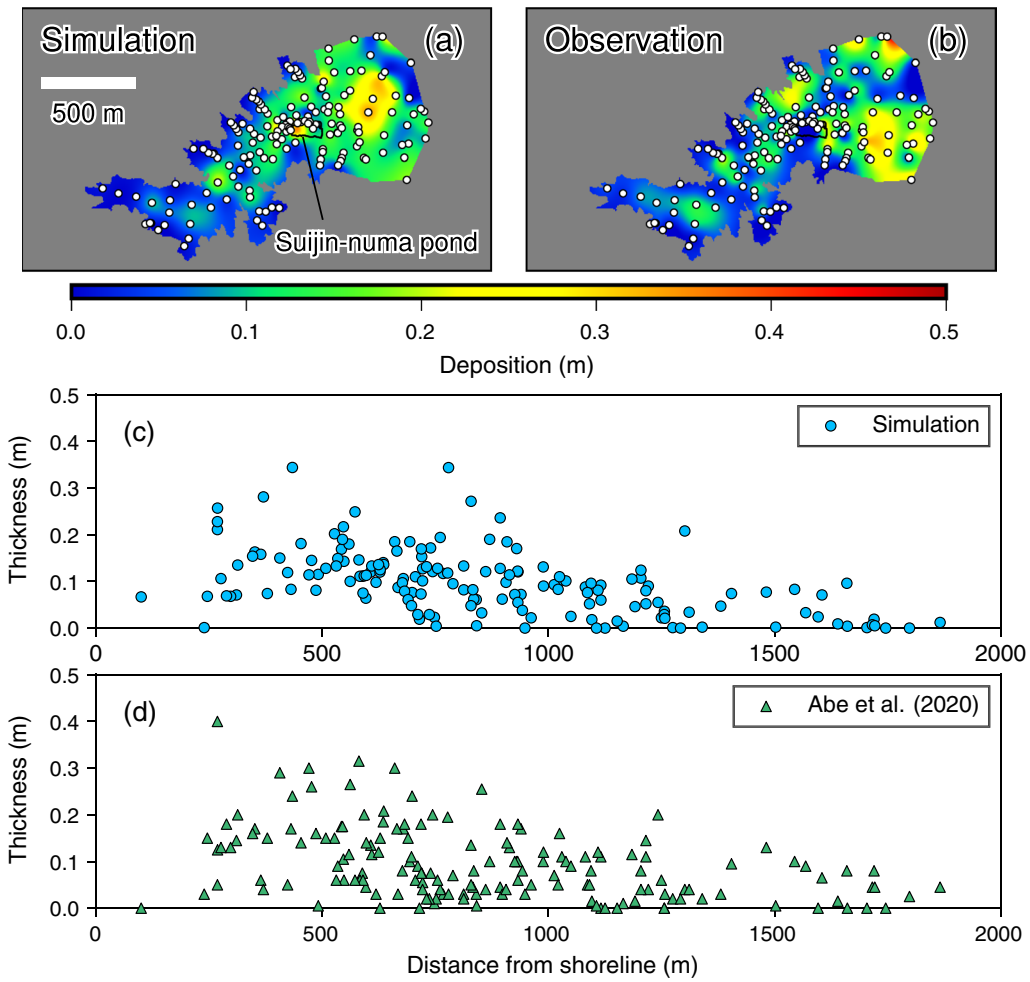

Fig. 2 Observed deposition and results of the sediment transport simulation for model and parameter validation (i.e., the reference simulation). **a** Thickness of the resampled and interpolated thickness based on the simulation. **b** Interpolated sand thickness distribution around the Suijin-numa pond. Thickness data were collected by Abe et al. (2020). **c** Shore-normal distribution of the simulated deposit thickness on the survey sites of Abe et al. (2020). **d** Shore-normal distribution of the observed deposit thickness (modified after Abe et al. 2020)

of tsunami deposits were underestimated (Additional file 1: Fig. S2), suggesting that a positive calibration of the boundary condition was necessary to fit the simulations to the observations. A calibrated simulation, in which the flux was increased to 115%, was performed, considering the K value of the preliminary result; consequently, an improved result with $K = 0.99$ and $\kappa = 1.24$ was acquired after comparing 77 trace height sites that met the reproducibility criteria ($0.95 < K < 1.05$ and $\kappa < 1.45$; Japan Society of Civil Engineers 2002). The calibrated simulation results were used for the reference simulation in the source modeling.

3.2.3 Fault model and sensitivity to subfault location

We used a set of subfaults (S1–S10) to consider slip heterogeneity (Fig. 1b). The geometries of the subfaults of a simple multi-segment fault model (Hayashi and Koshimura 2012) were adopted as an interplate fault plane along the Japan Trench because the subfault segmentation of Satake et al. (2013) is extremely fine and deposit-based source estimation could not accurately estimate the source location and slip distribution. The fault model of Hayashi and Koshimura (2012) was modified from the model originally proposed by Imamura et al. (2011) based on the aftershock distribution of the 2011 Tohoku earthquake (Nettles et al. 2011; Asano et al. 2011). The fault plane was divided into 10 subfaults having both lengths and widths of 100 km. Hereinafter, all source models were assumed to have a pure reverse faulting mechanism and a rise time of 30 s. Crustal deformation was calculated according to Okada

(1985) without considering the effects of the horizontal motion of the trench slope (Tanioka and Satake 1996).

The modeled rupture area extended 500 km and 200 km in the N–S and E–W directions, respectively. The slip distribution of the entire tsunami generation region could not be potentially recovered based on the tsunami deposit data acquired only from the study area. Thus, to clarify the contribution of each subfault to the study area, tsunami propagation, inundation, and sediment transport due to each subfault were simulated individually. A unit slip of 10 m was assigned to a subfault, and the slips for the remaining subfaults were set to zero. Simulations by each subfault were compared to identify major contributing subfaults, which were then used for estimating fault slip based on the comparison of the simulated and observed volumes of the tsunami deposits. We evaluated the sensitivity of each subfault based on the total deposition volume within Domain R6 (including the seafloor), since the inundation and onshore deposition are often minor in this sensitivity analysis.

Simulated deposit volume was sensitive to the distance to subfaults that acted as tsunami sources (Fig. 3). Deposit volumes by the shallower subfaults near the trench axis (S1–S5; Fig. 1b) were 44–388% more than those by the deeper subfaults near the shore (S6–S10) on the same latitude. The maximum deposition (317,433 m^3) was calculated using the shallower S4 subfault, whereas the minimum deposition (3753 m^3) was calculated using the deeper S6 subfault. Deposit volumes by the shallower S3 and S5 subfaults (85,837 m^3 and 87,833 m^3, respectively) were less than one-third of the adjacent S4; similarly, the deposit volumes by S8 and S10 (33,764 m^3 and 30,772 m^3, respectively) were nearly one-seventh of S9 (221,114 m^3). These results suggested that the volumes of the tsunami deposits could be explained primarily according to the slips on S4 and/or S9, which are located southeast, offshore of the study area.

3.2.4 Sediment transport simulations with varying slips

Changes in the deposit volume with varying fault slips were further examined for subfaults S4 and S9 in a total of 14 different rupture patterns. Since S4 has the largest sensitivity, estimation of the S4 slip was prioritized. The minimum fault slip for S4 and S9 was set to 10 m and 5 m, respectively, while a < 5 m slip indicated that the slip was absent on the subfault. Maximum fault slips for S4 and S9 were set to 40 m and 10 m, respectively, considering the slip distribution in Hayashi and Koshimura (2012). This assumption was generally consistent with other fault models of the 2011 Tohoku-oki earthquake (Satake et al. 2013; Yamazaki et al. 2018). Although the large slips (> 40 m) in previous models occurred on several narrow subfaults, in this study, such slips will be expressed as an averaged smaller slip within a large subfault instead of the impulsive slip distribution.

3.2.5 Sensitivity analysis on grain size

The TUNAMI-STM code approximates a single grain-size class of sediments. However, real tsunami deposits consist of different grain-size distributions. In the present study area, the median grain size of the tsunami deposits ranges from 1.3 ϕ to 2.6 ϕ (Abe et al. 2020). This can

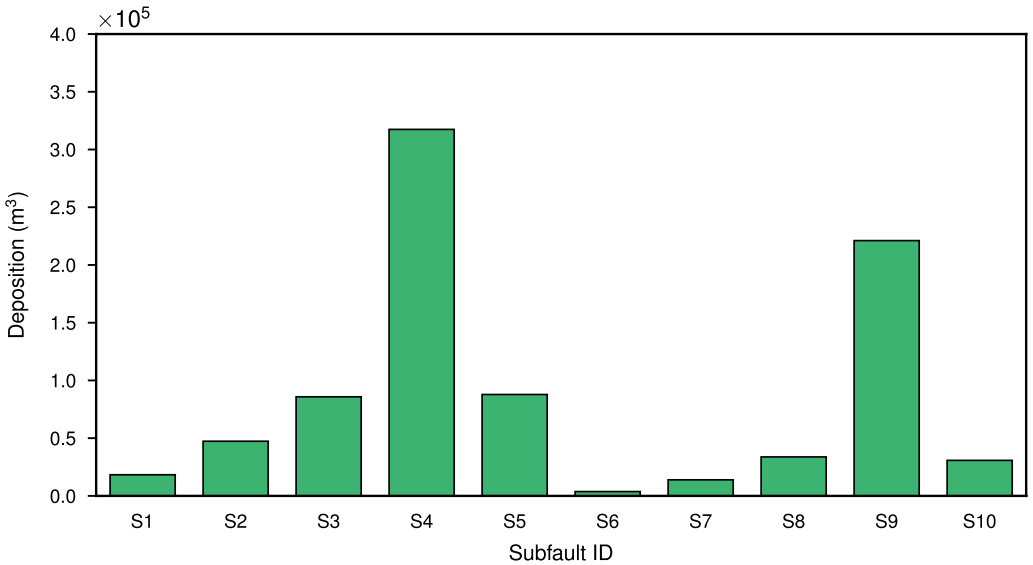

Fig. 3 Deposition associated with the individual subfault models. Uniform slip of 10 m is assumed for each subfault. Whole deposition volume in Domain R6 is displayed

result in uncertainty in tsunami sediment transport simulations. Ultimately, the uncertainty could propagate to the estimated fault slip because its estimation was based on the comparison between the simulated and observed deposit volumes.

Thus, a sensitivity analysis of grain size was conducted to evaluate the uncertainty in source modeling. The grain size was set from 70 to 130% of the reference value (0.267 mm) with a 10% interval. Grain-size-dependent parameters, such as settling velocity in still water, critical friction velocity, and empirical grain-size-dependent parameters, α and β for transport formulas, were recalculated using the grain size in each case. The parameters, α and β, were calculated by the following approximations (Masaya et al. 2020):

$$\alpha = 9.8044\ e^{-3.366d}$$

$$\beta = 0.0002\ e^{-6.5362d}$$

where d indicates the grain size. Moreover, the source model proposed by Satake et al. (2013) with the calibration was employed for the sensitivity analysis.

4 Results

4.1 Tsunami inundation and deposition from calibrated simulation

Calibrated numerical results on tsunami height and morphological changes are shown in Fig. 4. The tsunami height exceeded 8 m at the center of the study area (Fig. 4a). Additionally, the tsunami extensively inundated the valley floor where the Suijin-numa pond was located. The simulated inundation limit was consistent with the observed limit reported by Haraguchi and Iwamatsu (2013). Erosion due to the tsunami inundation was concentrated near the coastline (Fig. 4b); additionally, alongshore and cross-shore erosion types were identified. Alongshore erosion, which occurred near coastal dikes, showed a width of ~100 m and a depth of ~1 m, whereas cross-shore erosion was observed on the beach

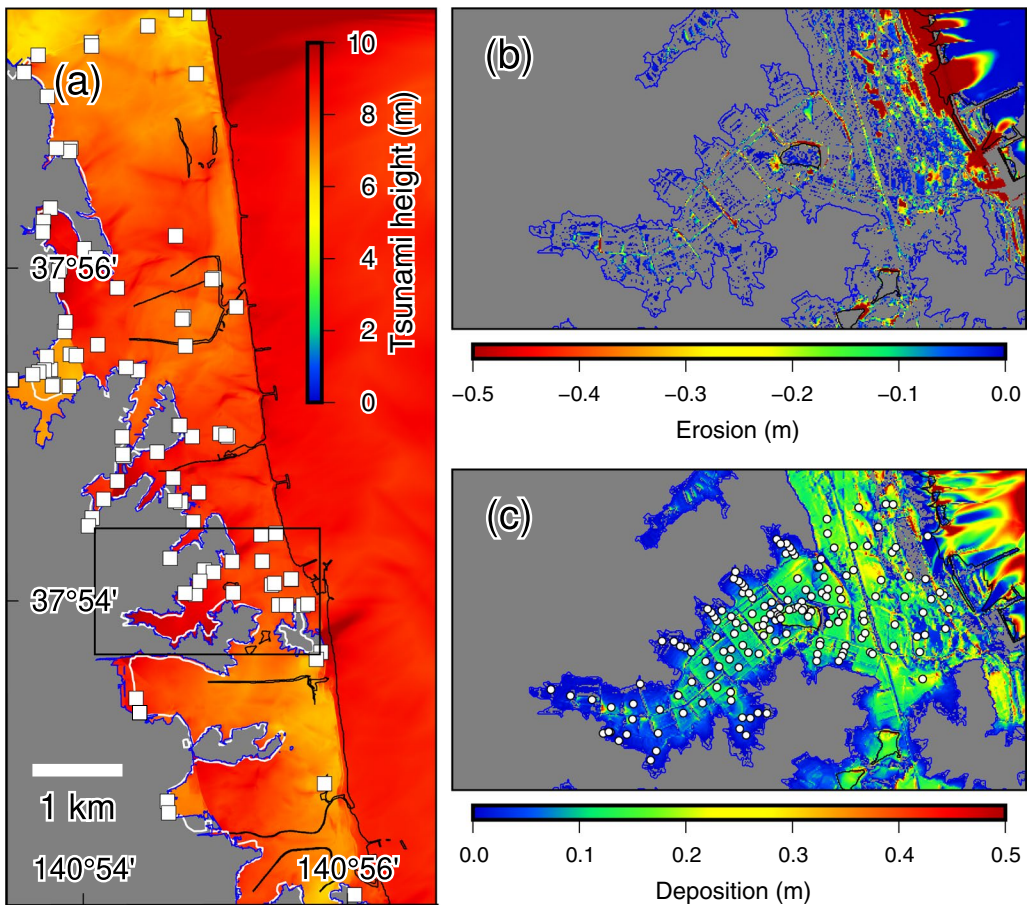

Fig. 4 Results of the reference simulation. **a** Distribution of the maximum tsunami height in Domain R6. Blue and white lines represent simulated and observed inundation limits, respectively. Black frame shows the spatial range of Fig. 2b and c. **b** Distribution of erosion depth near the Suijin-numa pond. Black line indicates the 0 m contour after the simulation. **c** Distribution of deposition thickness

and shallow sea floor near the breached coastal dikes. Further, on the backland, several erosion lines were recognized along road embankments. Simulated deposits were relatively thin on the shore and thick on the shallow sea bottom (Fig. 4c). Similar to erosion, abrupt changes in deposit thickness along the embankments were identified (Fig. 4c).

The simulated deposit volume (V_{sim}; Fig. 2a) was 86,645 m^3, which was consistent with the observed deposit volume $\left(V_{obs} = 85,336\ m^3\right)$. The simulated deposit was distributed approximately 1900 m from the coastline with a maximum value of ~0.4 m at 434 m from the coastline (Fig. 2c). Simulated deposit distribution (Fig. 2a and c) indicated that the deposit was thicker on the seaward of the Suijin-numa pond. The thickness of simulated deposits was generally thin inside the valley and increased locally. The observed thickness distribution was generally comparable with the simulated result (Fig. 2b). However, the locations of the thick deposits on the seaward of the Suijin-numa pond differed in the simulations and observations. In particular, the deposit thickness in the Suijin-numa pond in the observations was almost zero, whereas it was relatively more in the simulations. Although a significant scatter was observed, the simulated deposit thickness decreased with increasing distance from the coast (Fig. 2c). Generally, the shore-normal distribution of the simulated deposit thickness is comparable with the observed thickness (Abe et al. 2020; Fig. 2d).

4.2 Sediment transport simulations with varying fault slips

Figure 5 compares the deposit volumes estimated based on the field data and the results of the sediment transport simulations. Owing to large slips on both S4 and S9, the volume of deposition in the study area was also large. To explain the observed deposition (85,336 m^3), slip amounts of over 35 m and 5 m were required for S4 (se3510) and S9 (se4005), respectively (Fig. 5). Even if an exclusive slip of 40 m is assumed on S4, without a slip on S9, the simulated deposit volume was 78% of the observed volume, indicating that large slip is required on the deeper subfault S9. Results of the source models, se1010 and se1005, suggested that a combination of ~10 m slip near the trench axis and 5–10 m near the shore could not facilitate the formation of tsunami deposits in the study area (Fig. 5).

4.3 Sensitivity analysis of grain size

Figure 6 compares the shore-normal distribution of the simulated tsunami deposit thickness across varying grain sizes. At ~780 m from the shoreline, the maximum and average deposit thicknesses of fine grain size (0.187 mm, which is 70% of the reference size; Fig. 6a) were 0.36 m and 0.13 m, respectively, while those of coarse grain size (0.347 mm, which is 130% of the reference size; Fig. 6b) were 0.30 m and 0.07 m, respectively. Comparing Fig. 6a and b, the landward thinning trend is more notable with the coarser grain size. The sensitivity analysis results also showed a significant change in the depositional volume corresponding to the different grain sizes (Table 1). At a grain size of 0.187 mm, the deposition volume increased to 131% of the reference simulation, whereas as the grain size increased to 0.347 mm, the deposit volume reduced to 72% of the reference simulation.

5 Discussion

5.1 Validation of the tsunami sediment transport simulation

To better simulate tsunami-induced sediment erosion, transport, and resulting morphological changes, an accurate reproduction of tsunami hydrodynamics (e.g., tsunami height, waveform, and flow velocity) is necessary. The tsunami source model used in this study (Satake et al. 2013) could reproduce the observed tsunami waveforms at offshore stations and coastal tide gauges. However, these tsunami records were sparsely distributed spatially; additionally, coastal inundation was highly dependent on the resolution of the DEM used for the simulation. Thus, the validity of the tsunami source model does not necessarily guarantee a successful prediction of coastal inundation by a high-resolution simulation. Therefore, the simulation was calibrated with a flux factor of 115% based on the comparison results of the simulated and measured tsunami heights (Mori et al. 2012). Consequently, the simulated tsunami heights were close to the observations (see Sect. 3.2.2 and Additional file 1: Fig. S1). Additionally, the calibrated simulation well reproduced the observed inundation limit (white line in Fig. 4a; Haraguchi and Iwamatsu 2013).

Nevertheless, a better hydrodynamic simulation does not necessarily indicate a successful reproduction of sediment transport and sediment transport simulations must be validated through comparisons with field measurements. However, a point-by-point comparison is not feasible considering the local variability of deposit thickness, which cannot fully be addressed during the field observations. Thus, we compared the simulated and observed depositional volumes that could serve as a robust metric for validating the simulations.

The simulated deposition volume $\left(V_{sim} = 86,645\ m^3\right)$ was almost consistent with the observed deposition volume $\left(V_{obs} = 85,336\ m^3\right)$, indicating that the magnitude of sediment transport was correctly simulated in the reference simulation. The overall deposition trend in both simulations and observations was similar, except in the Suijin-numa pond (Fig. 2). Qualitatively, the

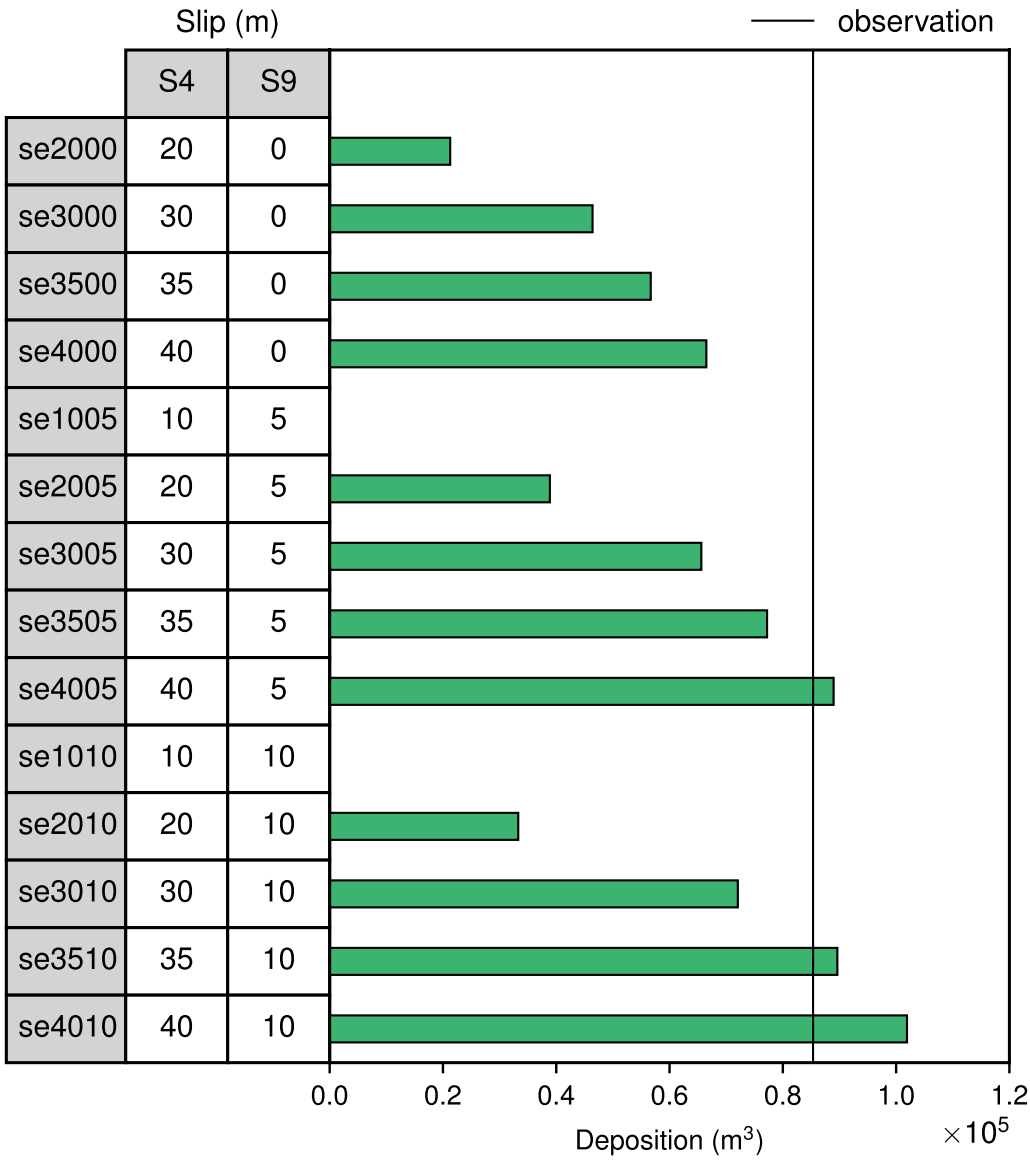

Fig. 5 Calculated deposition volumes from 14 models with varying fault slips on subfaults S4 and S9. Hypothetical models se3510 and se4005 well reproduced the depositional volume estimated based on the observation; black line (Abe et al. 2020)

observed (Abe et al. 2020; Fig. 2d) and simulated (Fig. 2c) shore-normal thickness distributions were similar. Further, the simulation demonstrated that the erosion due to the tsunami devastated the beach (Fig. 4b), and the cross-shore erosion changed the coastline significantly. Previous studies deduced that the concentrated backwash eroded the beach deposits, and the scour, similar to a small bay (so-called tsunami bay), remained even after the tsunami (Yoshikawa et al. 2015, 2017, 2018; Abe et al. 2020). Specifically, the simulation results indicated that the concentrated erosion on the beach was qualitatively consistent with such a deduction. Based on these quantitative and qualitative comparisons of the deposition volumes, the calibrated tsunami sediment transport simulation successfully reproduced the general characteristics of the tsunami inundation and sediment deposition, thus suggesting the possibility of investigating the tsunami source based on the simulated deposit volume. Despite the successful reproduction of the onshore deposition, the simulated volume of the beach erosion was 6.85×10^4 m^3, whereas the observed erosion volume was 1.34×10^5 m^3 (Abe et al. 2020). Considering the consistency in onshore deposition, this difference in erosion may influence the offshore rather than the onshore deposition

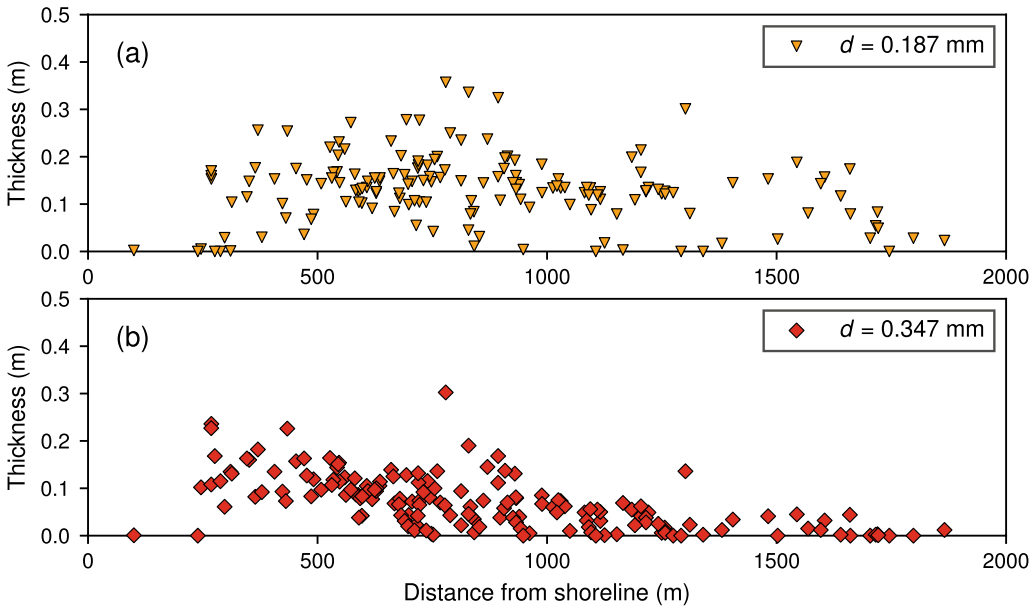

Fig. 6 Grain-size-dependent changes of the shore-normal distribution of simulated tsunami deposits. **a** Results of the finest ($d = 0.187$ mm) and **b** coarsest grain size ($d = 0.347$ mm)

Table 1 Summary of the sensitivity analysis of the grain size

d (mm)	w_0 (m)	u_c (m)	α	β	V_{sim} (m^3)	R_d (%)
0.187	0.02136	0.01463	5.22	5.89×10^{-5}	113,591	131
0.214	0.02576	0.01498	4.77	4.94×10^{-5}	99,161	114
0.240	0.02983	0.01528	4.37	4.17×10^{-5}	92,180	106
0.267	0.03386	0.01556	4.0	4.4×10^{-5}	86,645	100
0.294	0.03768	0.01582	3.64	2.93×10^{-5}	78,493	91
0.320	0.04116	0.01605	3.34	2.47×10^{-5}	70,573	81
0.347	0.04458	0.01628	3.05	2.07×10^{-5}	62,687	72

d, Grain size; w_0, Settling velocity in the static water column; u_c, Critical shear velocity; α, Empirical parameter for the bedload formula; β, Empirical parameter for the exchange rate formula; V_{sim}, Volume of resampled and interpolated deposit around Suijin-numa; R_d, Ratio of deposition volume to the reference ($d = 0.267$ mm) result

process. Thus, the results of the calibrated tsunami sediment transport simulation can be regarded as valid as long as it is focused on the onshore deposition.

5.2 Tsunami source model inferred from the tsunami deposit and its source

Among the models se3510 and se4005, it is difficult to judge based solely on the deposit volume which is the better one because both models well reproduce the deposition volume (Fig. 5). Even if measured tsunami heights are available, the judgment is still uneasy because the difference in the K (1.15 for se3510 and 1.13 for se4050) and κ (1.21 for se3510 and 1.22 for se4050) metrics is quite small. Similarly, the comparison of the inundation limit is not promising to find their difference (Fig. 7). Therefore, another metric other than those is necessary to further constrain the tsunami source.

Masaya et al. (2021) highlighted that simulated sediment source provides additional information to estimate paleotsunami sources. They proposed the ratio of marine-origin deposits to whole deposits, P_{sea}, as defined:

$$P_{sea} = \frac{V_{sea}}{V_{all}}$$

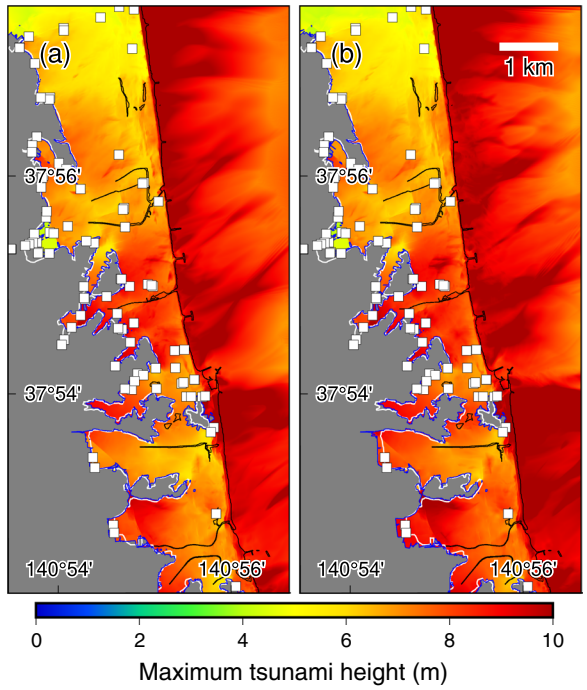

Fig. 7 Distributions of the maximum tsunami height attributed to **a** se3510 and **b** se4005. White and blue lines indicate the observed and simulated inundation limits

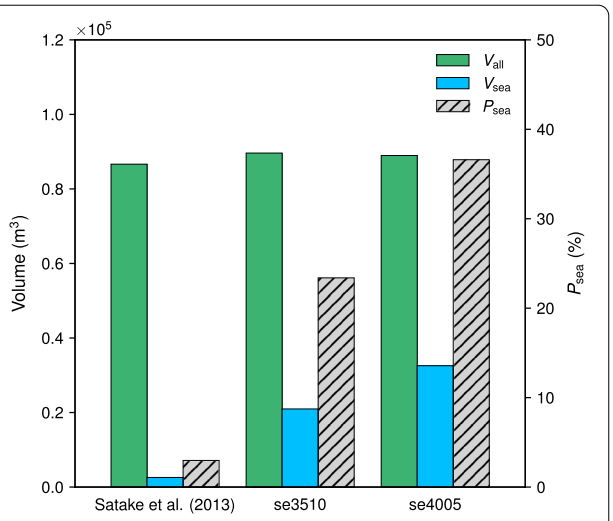

Fig. 8 Volumes of the whole deposits (V_{all}) and marine-origin deposits (V_{sea}) around the Suijin-numa pond (simulated according to the method by Masaya et al. 2021). Ratios $P_{sea} = V_{sea}/V_{all}$ for each case are shown

where V_{sea} and V_{all} denote the volumes of marine-origin deposits and whole tsunami deposits in the area of comparison, respectively. A numerical experiment shows that the P_{sea} ratio varies depending on the tsunami waveform and can be a constraint of deposit-based tsunami source modeling (Masaya et al. 2021). In the present approach of Eulerian simulations, exact value of V_{sea} cannot be calculated directly. Thus, V_{sea} was approximated based on the deposit volume calculated assuming that the entire land is non-erodible.

Although an exact P_{sea} may not be obtained from real tsunami deposits, contributions of different sediment sources can be elucidated by detailed analyses. The sandy tsunami deposits in the Sendai Plain formed by the 2011 Tohoku-oki tsunami have been estimated to originate onshore (Szczuciński et al. 2012; Takashimizu et al. 2012; Putra et al. 2013). For example, marine diatom species occupy only ~2% of the entire diatom assemblage in the sandy fraction of the tsunami deposits in the northern Sendai Plain (Takashimizu et al. 2012). Existing tsunami sediment transport simulations support such micropaleontological findings (Sugawara et al. 2014b). In the present study area, Abe et al. (2020) elucidated the onshore source of the tsunami deposits by comparing pre- and post-tsunami DEMs and grain-size distributions of the deposits. P_{sea} in the reference simulation is only 3% (Fig. 8), which fits the estimation by Abe et al (2020).

Deposit distributions are in general similar among the models se4005 and se3510 (Fig. 9). However, seafloor erosion near the coastline differs significantly. In the case of se4005 (Fig. 9c), a shore-parallel band of seafloor erosion was found ~ 200 m offshore of the coastline, whereas such a band was located much closer to the land and was relatively narrow in se3510 (Fig. 9a). The difference in offshore erosion can affect the contribution of the marine sediment (i.e., P_{sea}). Figure 8 shows that se4005 shows a greater contribution ($P_{sea} = 37\%$) comparing with se3510 ($P_{sea} = 23\%$).

Figure 10 compares the tsunami waveforms by three different source models (Satake et al. 2013, se3510, and se4005) at a virtual tide station SJN1 (Fig. 1). The waveforms by the models se3510 and se4005 are in general similar, except for a period between 45 and 63 min. Among a whole range of waveforms, se3510 and se45005 have different features compared to Satake et al. (2013). Major differences are the duration of the main wave and its precedent sea-level drop. With hypothetical source models, an abrupt sea level drop (receding wave 45–63 min) occurred prior to the arrival of the main wave. The simulation by model se4005 yielded a larger receding wave compared with that by se3510. In the reference model (Satake et al. 2013), a gradual and moderate decrease in the sea level appeared prior to the main wave. Masaya et al. (2021) pointed out that the period of the main wave and the amplitude of the precedent receding wave control the erosion of the shallow seafloor.

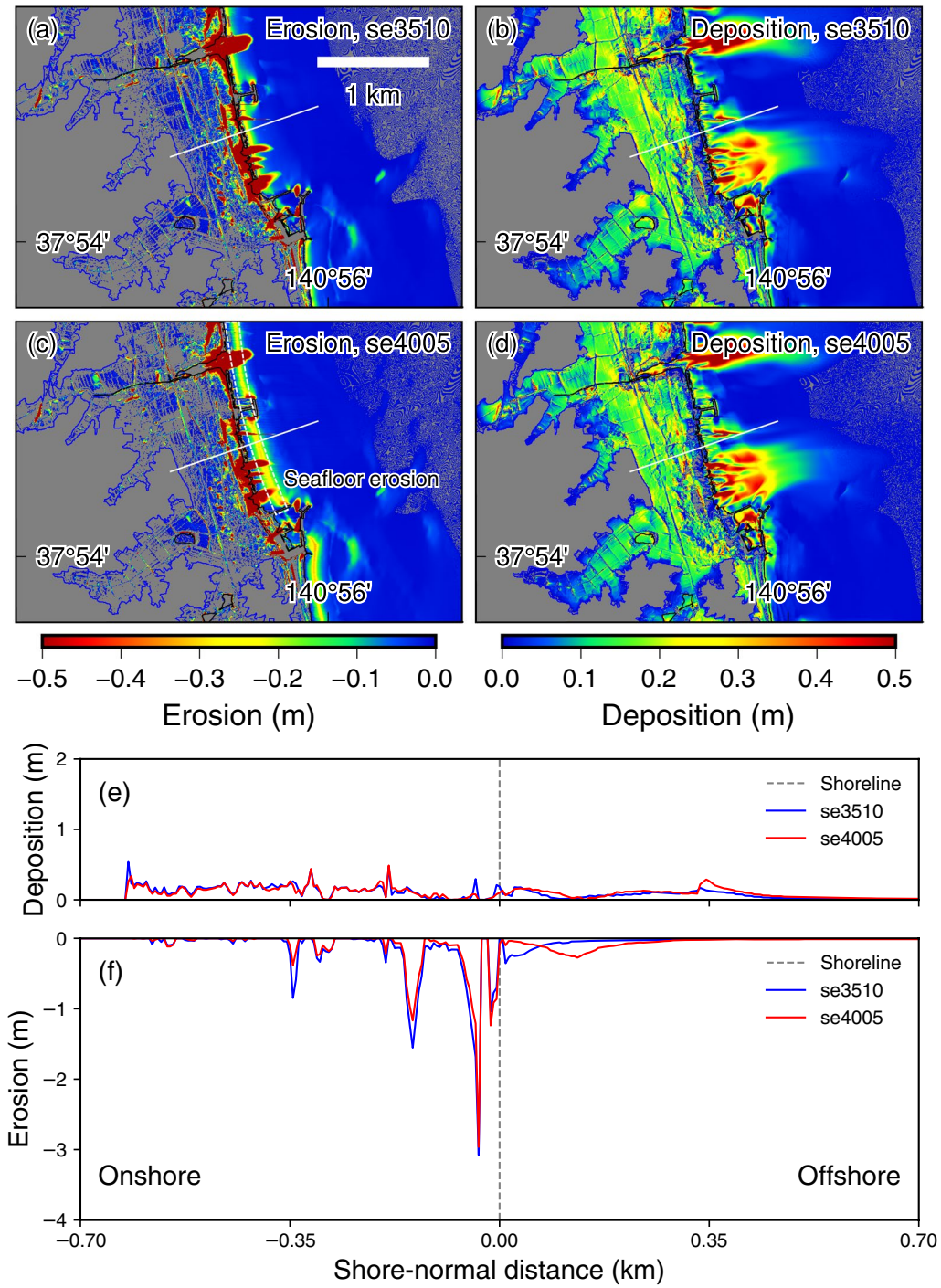

Fig. 9 Results of the sediment transport simulation using the source models, se3510 (**a** and **b**) and se4005 (**c** and **d**). Morphological changes (negative and positive values indicate erosion and deposition, respectively) around the Suijin-numa pond are displayed. Black lines represent post-tsunami 0 m contours for each scenario. (**e**) Deposition trend of these scenarios along the transect are shown in (**a**–**d**) as a white line. (**f**) Erosion trends along the same transect as (**e**)

With a larger precedent receding wave, nearshore seafloor is exposed extensively and the main wave with a longer period exerts a persisting bottom shear stress on the seabed, resulting in greater sediment erosion and entrainment into the flow.

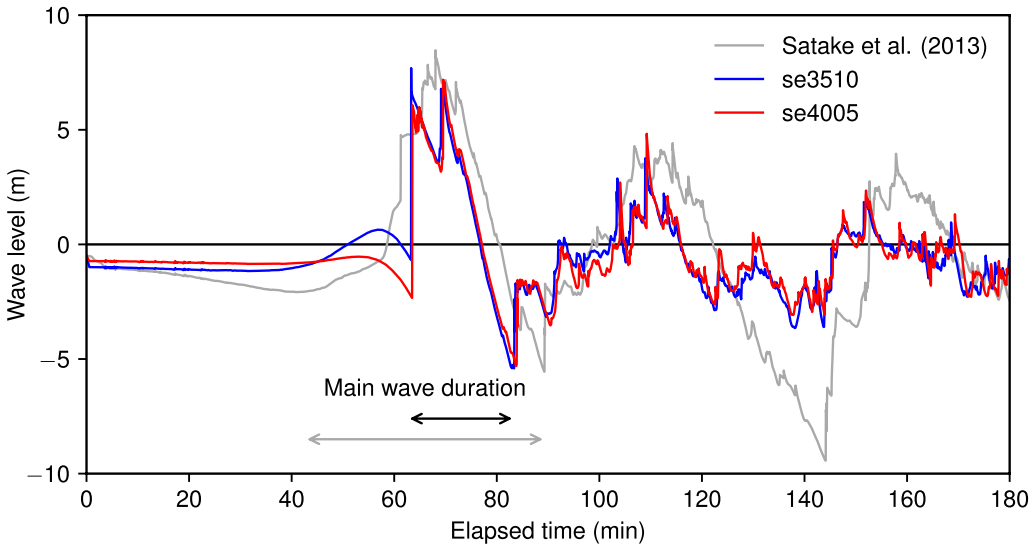

Fig. 10 Waveforms recorded on a virtual tide station, SJN1. Along with scenarios se3510 and se4005, a waveform associated with the source model of Satake et al. (2013) is shown as a reference. Black and gray arrows indicate the duration of the main wave associated with hypothetical models (se3510 and se4005) and the reference simulation, respectively

Considering the minor contribution of seafloor sediments (Abe et al. 2020), simulations with a lower P_{sea} value are preferable. Thus, the model se3510 better explains the sediment source of the 2011 Tohoku-oki tsunami deposits in the study area. Note that P_{sea} of the hypothetical models is much higher than that of the reference simulation ($P_{sea} = 3\%$). The hypothetical models may have a limitation on the reproducibility of the waveforms and resulting P_{sea} due to their insufficient spatial and temporal resolution of the slip distribution.

The above approach to constrain the tsunami source model based on P_{sea} relies on the assumption that differences between beach and shoreface deposits can be identified and fractions of respective deposits can be quantified. Distinguishing the deposits based on geological proxies is difficult because the differences may not be evident in general cases as the littoral drift system mixes and homogenizes these deposits. Therefore, to apply P_{sea} for general cases, a new methodology to quantify fractions of beach and shoreface deposits is required.

5.3 Comparison with existing source models

Figure 11 compares the slip models inferred from this study and previous studies. Iinuma et al. (2012), Satake et al. (2013), and Yamazaki et al. (2018) estimated the slip distribution based on geodetic inversion, tsunami inversion, and a combination of iterative forward modeling of tsunamis and inversion of teleseismic *P*-waves, respectively. The fault model of Yamazaki et al. (2018) represents a self-consistent slip that can explain seismic and tsunami waveforms and tsunami inundation. In this study, the slip distribution estimated based on the tsunami deposits (se3510; Fig. 11a) showed a larger slip on S4 near the trench axis than in other models. Conversely, the slip amount on the landward S9 was consistent with that in the other models. Although the slip amount is smaller than that near the trench axis, a "deep large slip" (Satake et al. 2013), shown as subfaults surrounded by a thick frame in Fig. 11, is necessary to explain the deposit volume in the study area. This was consistent with the results of Satake et al. (2013), who indicated the significant contribution of the "deep large slip" to the extended inundation in the Sendai Plain.

Satake et al. (2013) also reported that the "shallow huge slip" near the trench axis does not influence the inundation in the Sendai Plain. In fact, the tsunami sediment transport simulation based on the source model proposed by Satake et al. (2013) without the "shallow huge slip" can explain not only the observed inundation but also deposit volume (Additional file 1: Fig. S3). Here, the question that arises is whether the deposit-based fault model se3510 was inconsistent with the findings of Satake et al. (2013). In this study, the assumption of different ranges of slips on deep (0–10 m) and shallow (0–40 m) subfaults was used for slip estimation, based on the slip distributions of the 2011 Tohoku-oki earthquake determined by Hayashi and Koshimura (2012), which attributed larger slips to the shallow subfaults. If the ranges of the slip to be tested are not constrained based on the existing fault

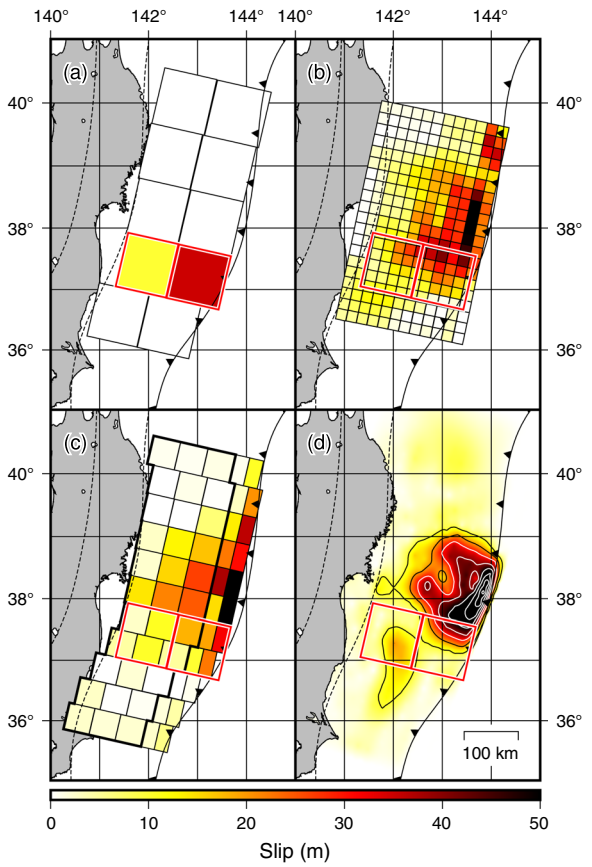

Fig. 11 Slip distribution models of the 2011 Tohoku-oki earthquake. Red frames represent the projected shapes of subfaults S4 and S9. Plate boundary was retrieved by Iwasaki et al. (2015). **a** Source model se3510. **b** TP-MOD based on iterative forward tsunami simulation and teleseismic inversion by Yamazaki et al. (2018). **c** Slip distribution inferred by tsunami waveform inversion (Satake et al. 2013). Thick-framed subfaults belong to the "deep slip"; other subfaults belong to the "shallow slip." **d** Slip distribution proposed according to an inversion of geodetic observation by Iinuma et al. (2012)

model, the balance of the estimated slip on the deep and shallow subfaults may differ. Thus, in this study, the empirical assumption of the slip range may have resulted in the selection of the slip distribution with a larger shallow slip. In addition to the assumption about the maximum slip, the subfault size might explain this conflict. Here, only a seaward half of subfault S4 belongs to the "shallow slip" domain defined by Satake et al. (2013). A combination of narrow and wide subfault in shallow and deep parts, respectively (an example can be found in Ioki and Tanioka 2016), may be more suitable for this kind of discussion.

Compared with se3510, se4005 had a slip distribution that was larger on S4 and smaller on S9. This implies that the larger slip on the landward S9 (se3510) contributed to the smaller receding wave (Fig. 10). A huge slip near the trench axis caused significant subsidence of the sea floor and the sea surface landward of the rupture area (Satake and Tanioka 1999). However, with a larger slip on the deep portions of the plate interface, such negative sea surface displacement is negated due to larger crustal uplifting directly below. Thus, the smaller amount of marine-origin materials in the onshore tsunami deposit by the se3510 source model can be associated with the larger slip on Subfault S9 and the resulting smaller receding wave near the coastline.

Ignoring the contribution of other subfaults might affect the slip amounts on S4 and S9. In fact, S3, which is equivalent to the segment with the largest slip during the Tohoku-oki earthquake, was located directly north of S4. Although the sensitivity of the fault slip to the deposit volume in the study area was low, a huge slip (over 30 m) on S3 similar to previous models may affect the sediment erosion and deposition in the study area and reduce the slip amount on S4. However, without any prior knowledge of the slip distribution, it may be difficult to assume such a distant large slip in a paleoseismic event. The paleotsunami source model as well as se3510 (Fig. 11a) can be incomplete if reconstruction relies on spatially limited tsunami deposit data.

It is noteworthy that se3510 is a solution based on several assumptions from the result of the sensitivity analysis and known general along-dip slip distribution. In this study, the optimal solution seemed not to be determined without any a priori assumptions because the geological data for tsunami source modeling are quite limited. Two problems in this study, the incomplete spatial extent of the reconstructed source and strong dependency on the assumptions, may be conquered by using extensive geological data along the tsunami-prone coast. The estimation of the slip on each subfault can also be more accurate by properly solving trade-off relationships among all subfault slips in the source region. Thus, for better deposit-based tsunami source modeling, the availability of tsunami deposit data from a wide area along the tsunami-prone coast is essential.

5.4 Uncertainty in deposit-based source estimation

Various factors, such as inputs and model setups, associated with tsunami sediment transport modeling can introduce uncertainties in the numerical simulations (Jaffe et al. 2016; Sugawara 2019). The results of the simple sensitivity analysis (Table 1) showed the fluctuated simulated deposit volume with changes in grain size. In general, the grain size of the sediment source is difficult to constrain despite its importance in the simulations.

Figure 12 demonstrates that the uncertainty in grain-size setting propagated via the numerical simulation to the estimated fault slip. With a fixed fault slip, the deposit volume was ~15,000 m^3 smaller for every 0.05 mm increase in the grain size. Such a change was nearly equivalent to the variations in the deposit volume, due to a decrease in the fault slip on S4 by ~4.3 m with the fixed grain size. Although it is just an example, this comparison indicated that the uncertainty due to sediment grain size should be carefully considered in paleotsunami source estimation.

5.5 Implications for paleotsunami studies

Deposit-based source modeling requires the accurate simulation of tsunami deposit formation at surveyed sites. The bottom deposits of coastal ponds and lakes are important candidate sites for field surveys in paleotsunami research due to the high preservation potential of tsunami deposits (Sawai et al. 2008; Furumura et al. 2011; Kempf et al. 2017). Previously, the bottom sediments of the Suijin-numa pond have been surveyed to investigate the paleotsunami history (Sawai et al. 2008). Thus, the successful simulation of lake-bottom tsunami deposit formation will greatly contribute to the assessment of tsunami magnitude. Despite this importance, the simulated thickness distribution in the Suijin-numa pond was significantly different from the observed distribution even in the reference simulation (Fig. 2). This could be caused by the limitation of 2DH hydrodynamic simulation (TUNAMI-N2), which cannot simulate three-dimensional flow and the resulting sedimentary process. Thus, this limitation will hinder the application of such numerical models in paleotsunami source estimation based on lake-bottom tsunami deposits.

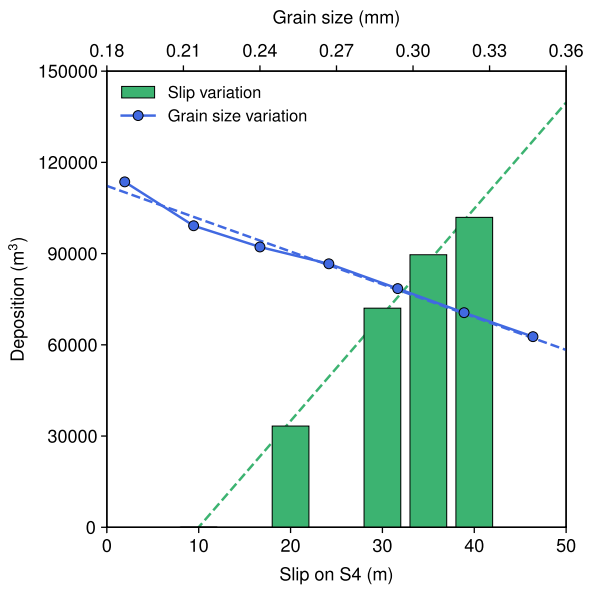

Fig. 12 Comparison of changes in the deposition volume with variations in slip on S4 (with fixed slip of 10 m on S9) and grain size. Dashed lines indicate linear approximations of the data shown in the same color

Regarding the paleotsunami source modeling, we have more difficulties than in this study. Available data for inputs, such as topography, land condition, and initial tide level, can be poorly constrained. Moreover, post-depositional processes can modify the thickness of tsunami deposits, leaving them unidentifiable near the distribution limit (Szczuciński 2012; Spiske et al. 2020). Even if deposits can be identified, the consolidation of tsunami deposits can decrease the deposit thickness and volume and cause an underestimation of the slip. These uncertain inputs, boundary conditions, and constraints hinder the accurate estimation of a paleotsunami source. Thus, the uncertainty in the estimated source should be demonstrated even though the estimation appears to be successful.

The combination of forward and inverse models (i.e., hybrid modeling; Sugawara et al. 2014a; Jaffe et al. 2016) is a promising approach for deposit-based tsunami source modeling. Inverse models of tsunami-induced sediment transport (Jaffe and Gelfenbaum 2007; Tang and Weiss 2015; Naruse and Abe 2017) are useful to extract tsunami flow conditions, such as flow velocity, inundation depth, and concentration of suspended sediments, from sedimentary features of tsunami deposits. Inverse modeling is mainly a contrasting approach to forward modeling of tsunami-induced sediment transport (e.g., TUNAMI-STM), whereas hybrid modeling utilizes both models to complement each other; for example, forward simulation can be used to validate an assumption of the inverse model and inverse calculations can be used to estimate the hydraulic constraint of the forward model. Although the methodology is not yet established, this approach might be effective to mitigate the uncertainty of the tsunami source and the accurate estimation thereof.

Furthermore, considering the uncertainties of tsunami deposit characteristics, using the deposit thickness or volume as the only constraint of source estimation can create problems. Although difficult to implement, including constraints from various kinds of sedimentary data is a possible solution. In addition to thickness, volume, and sediment source, grain-size distribution of tsunami deposits may provide clues on the characteristics of the tsunami source (Gusman et al. 2018). Tsunami source modeling with sediment transport simulations has the potential to fully utilize such sedimentary data. Other paleoseismological information, such as coseismic crustal deformation and historical records, can be considered

as additional constraints (Sugawara et al. 2019; Dourado et al. 2021). Moreover, seismological scaling laws (Murotani et al. 2013; Skarlatoudis et al. 2016), which are empirical relationships between fault parameters, are useful to construct hypothetical fault models (Minamidate et al. 2022). Such additional constraints should be examined from the perspectives of both geology and numerical modeling.

6 Conclusions

This study examined the potential and limitations of tsunami source estimation based on the 2011 Tohoku-oki tsunami deposits collected from the southernmost part of the Sendai Plain. The tsunami sediment transport model was employed to fully utilize the observed sedimentary data. The sensitivity analysis conducted using single subfault models revealed that coseismic slips on only two out of ten subfaults could be reconstructed based on the tsunami deposits. We initially examined the hypothetical source model by comparing the tsunami deposit volumes. Two possible source models passed the selection and were further investigated. Based on the sediment source information, the source model, se3510, with slips of 35 m and 10 m on the shallow and deep parts of the fault, respectively, was preferred. Although the slip near the trench axis was larger than that of the previously proposed models, the results of source modeling showed that the slip distribution of the triggering earthquake could be estimated reasonably based on the tsunami deposits. Note that the optimal model se3005 relies on several assumptions to compensate poor spatial extent of geological data.

The application of the sediment transport simulations facilitated the direct comparison of the calculated sedimentary information (e.g., deposit thickness, volume, and source) with sedimentological observations and interpretation. In particular, the tsunami deposit volume was utilized as the primary constraint of source modeling, and the corresponding observation data were suitable for comparison. We also used the sediment source information, which was obtained using the sediment transport model as an additional constraint. Based on the trial-and-error approach and the additional constraint, an overestimated but comparable slip on the specific region of the megathrust was deduced. This result suggested that, even with high-quality data, the precise estimation of the slip based on tsunami deposits was difficult because of the dependence on the deposits in a limited area. Further, the entire depiction of a giant interplate earthquake from tsunami deposits can be time-consuming because it requires the compilation of sedimentary data from a wide area of the devastated coast and trial-and-error simulation throughout the dizzying array of hypothetical scenarios. However, the uncertainties of sedimentary data and the simulated result will make such attempts difficult. Thus, using additional constraints other than the deposit thickness or volume is one solution to improve the accuracy of paleotsunami source modeling.

Abbreviations

2DH: Two-dimensional horizontal; DEM: Digital elevation model; LiDAR: Light detection and ranging; STM: Sediment transport model; TP: Tokyo Peil.

Supplementary Information

The online version contains supplementary material available at https://doi.org/10.1186/s40645-022-00527-x.

Additional file 1: Fig. S1. Comparison of the scatter plot of the observed and simulated tsunami heights with and without the calibration of the boundary condition for the computational Domain R6. The original (not calibrated) tsunami source model is proposed by Sateke et al. (2013). Observational data were retrieved from Mori et al. (2012). The black line indicates a perfect agreement. **Fig. S2.** Characteristics of the sedimentary results of the simulation using the source model of Satake et al. (2013) without considering the calibration of the boundary condition to the computational Domain R6. **a** Distribution of deposition. The blue line shows the limit of the simulated inundation area, which was narrower than that after calibration (Fig. 2c). **b** Shore-normal distribution of deposit thickness with and without calibration. The thickness on most sites increased with the calibration. **Fig. S3.** Results of the sediment transport simulation using the deep slip model (subfaults on 2–4 columns defined in Satake et al. 2013; thick-framed subfaults in Fig. 10). **a** Distribution of erosion depth. **b** Distribution of deposition. Blue line represents the simulated inundation limit. Black dashed line represents the actual inundation limit reported by Haraguchi and Iwamatsu (2013). **c** Comparison of deposition volume. Even though there is no positive calibration of flux, the result from the deep slip model exceeds that from original model with the calibration (composite of deep and shallow slips).

Acknowledgements

We would like to thank the two anonymous reviewers and the associate editor Masaki Yamada for their constructive comments which improved this manuscript. DEMs used for constructing bathymetric and topographic data for numerical simulations were provided by the Geospatial Authority of Japan. The plate models by Iwasaki et al. (2015) were constructed using topographic and bathymetric data by the Geospatial Information Authority of Japan (250 m digital map), Japan Oceanographic Data Center (500-m mesh bathymetry data, J-EGG500, http://www.jodc.go.jp/jodcweb/JDOSS/infoJEGG_j.html), and Geographic Information Network of Alaska, University of Alaska (Lindquist et al. 2004). The Generic Mapping Tools version 6 (Wessel et al. 2019) was employed for data handling and constructing figures.

Author contributions

HM conducted numerical analyses and interpreted the results. DS proposed the topic, conceived, and designed the study and assisted in the result interpretation. TA and KG provided the observed sedimentary data and collaborated with the corresponding author in the writing of the manuscript. All authors read and approved the final manuscript.

Funding

This research was supported partly by the collaborative research project by the Shimizu Corporation and Tohoku University (FY2020–FY2022).

Availability of data and materials

The datasets used and/or analyzed during the current study are available from the corresponding author upon reasonable request.

Declarations

Competing interests

The authors declare that they have no competing interests.

Author details

[1]Department of Earth Science, Graduate School of Science, Tohoku University, 6-3 Aramaki Aza-Aoba, Aoba-ku, Sendai, Miyagi 980-8578, Japan. [2]International Research Institute of Disaster Science, Tohoku University, 468-1 Aramaki Aza-Aoba, Aoba-ku, Sendai, Miyagi 980-8572, Japan. [3]Geological Survey of Japan, National Institute of Advanced Industrial Science and Technology, 1-1-1 Higashi, Tsukuba, Ibaraki 305-8567, Japan. [4]Department of Earth and Planetary Science, The University of Tokyo, 7-3-1 Hongo, Bunkyo-ku, Tokyo 113-0033, Japan.

Received: 12 July 2022 Accepted: 27 November 2022
Published online: 05 December 2022

References

Abe T, Goto K, Sugawara D (2012) Relationship between the maximum extent of tsunami sand and the inundation limit of the 2011 Tohoku-oki tsunami on the Sendai Plain, Japan. Sediment Geol 282:142–150. https://doi.org/10.1016/j.sedgeo.2012.05.004

Abe T, Goto K, Sugawara D (2020) Spatial distribution and sources of tsunami deposits in a narrow valley setting: insight from 2011 Tohoku-oki tsunami deposits in northeastern Japan. Prog Earth Planet Sci 7:7. https://doi.org/10.1186/s40645-019-0318-6

Aida I (1977) Simulations of large tsunamis occurring the past off the Sanriku district. Bull Earthq Res Inst Univ Tokyo 52:71–101 (**In Japanese, with English abstract**)

Aida I (1978) Reliability of a tsunami source model derived from fault parameters. J Phys Earth 26:57–73. https://doi.org/10.4294/jpe1952.26.57

Arimitsu T, Matsuda S, Murakami Y, Shikata T, Kawasaki K, Mishima T, Shimizu R, Sugawara D (2017) Influence of computational parameters on accuracy of movable bed model for tsunamis. J Jpn Soc Civil Eng Ser B2 73:I_589-I_594. https://doi.org/10.2208/kaigan.73.I_589 (**In Japanese, with English abstract**)

Asano Y, Saito T, Ito Y, Shiomi K, Hirose H, Matsumoto T, Aoi S, Hori S, Sekiguchi S (2011) Spatial distribution and focal mechanisms of aftershocks of the 2011 off the Pacific coast of Tohoku Earthquake. Earth Planets Space 63:669–673. https://doi.org/10.5047/eps.2011.06.016

Butler R, Burney D, Walsh D (2014) Paleotsunami evidence on Kaua'i and numerical modeling of a great Aleutian tsunami. Geophys Res Lett 41:6795–6802. https://doi.org/10.1002/2014GL061232

Dourado F, Costa PJM, La Selle S, Andrade C, Silva AN, Bosnic I, Gelfenbaum G (2021) Can modeling the geologic record contribute to constraining the tectonic source of the 1755 CE Great Lisbon Earthquake? Earth Space Sci 8:e2020EA001109. https://doi.org/10.1029/2020EA001109

Fujita Y, Kano H, Takizawa F, Yashima R (1988) Geology of the Kakuda district (with geological sheet map at 1:50,000). Geol Surv Jpn. (**In Japanese, with English abstract**)

Fujiwara O (2008) Bedforms and sedimentary structures characterizing tsunami deposits. In: Shiki T, Tsuji Y, Yamazaki T, Nanayama F (eds) Tsunamiites: features and implications. Elsevier, Amsterdam. https://doi.org/10.1016/B978-0-444-51552-0.00004-7

Fujiwara O, Tanigawa K (2014) Bedforms record the flow conditions of the 2011 Tohoku-Oki tsunami on the Sendai Plain, northeast Japan. Mar Geol 358:79–88. https://doi.org/10.1016/j.margeo.2014.04.013

Furumura T, Imai K, Maeda T (2011) A revised tsunami source model for the 1707 Hoei earthquake and simulation of tsunami inundation of Ryujin Lake, Kyushu, Japan. J Geophys Res Solid Earth 116:B02308. https://doi.org/10.1029/2010JB007918

Goto C, Ogawa Y, Shuto N, Imamura F (1997) IUGG/IOC TIME project, numerical method of tsunami simulation with the leap-frog scheme. UNESCO, Paris

Goto K, Chagué-Goff C, Fujino S, Goff J, Jaffe B, Nishimura Y, Richmond B, Sugawara D, Szczuciński W, Tappin DR, Witter R, Yulianto E (2011) New insights of tsunami hazard from the 2011 Tohoku-oki event. Mar Geol 290:46–50. https://doi.org/10.1016/j.margeo.2011.10.004

Gusman AR, Goto T, Satake K, Takahashi T, Ishibe T (2018) Sediment transport modeling of multiple grain sizes for the 2011 Tohoku tsunami on a steep coastal valley of Numanohama, northeast Japan. Mar Geol 405:77–91. https://doi.org/10.1016/j.margeo.2018.08.003

Haraguchi T, Iwamatsu A (2013) Detailed maps of the impacts of the 2011 Japan tsunami, Revised edn. Kokon Shoin, Tokyo. (**In Japanese**)

Hayashi S, Koshimura S (2012) Measurement of the 2011 Tohoku tsunami flow velocity by the aerial video analysis. J Jpn Soc Civil Eng Ser B2 68:I_366-I_370. https://doi.org/10.2208/kaigan.68.I_366 (**In Japanese, with English abstract**)

Hisamatsu A, Imamura F, Matsu'ura RS (2017) The conical fault model for reproducing slip distribution and tsunami waveform of the 2011 off the Pacific Coast of Tohoku earthquake. J Jpn Soc Civil Eng Ser B2 73:I_295-I_300. https://doi.org/10.2208/kaigan.73.I_295 (**In Japanese, with English abstract**)

Hisamatsu A, Sugawara D, Goto K, Imamura F (2019) Tsunami source estimation for the 2011 off the Pacific coast of Tohoku Earthquake using thickness distribution of tsunami deposits in a wide area. J Jpn Soc Nat Disaster Sci 37:419–432. https://doi.org/10.24762/jndsj.37.4_419 (**In Japanese, with English abstract**)

Hori K, Kuzumoto R, Hirouchi D, Umitsu M, Janjirawuttikul N, Patanakanog B (2007) Horizontal and vertical variation of 2004 Indian tsunami deposits: An example of two transects along the western coast of Thailand. Mar Geol 239:163–172. https://doi.org/10.1016/j.margeo.2007.01.005

Iinuma T, Hino R, Kido M, Inazu D, Osada Y, Ito Y, Ohzono M, Tsushima H, Suzuki S, Fujimoto H, Miura S (2012) Coseismic slip distribution of the 2011 off the Pacific Coast of Tohoku Earthquake (M9.0) refined by means of seafloor geodetic data. J Geophys Res Solid Earth 117:B07409. https://doi.org/10.1029/2012JB009186

Imamura F, Koshimura S, Murashima Y, Akita Y, Shinya Y (2011) Tsunami simulation for the 2011 off the Pacific coast of Tohoku earthquake (Tohoku University Model version 1.1). https://www.tsunami.irides.tohoku.ac.jp/hokusai3/J/events/tohoku_2011/model/dcrc_ver1.1_111107.pdf. Accessed 6 Apr 2022. (**In Japanese, translated title**)

Ioki K, Tanioka Y (2016) Re-estimated fault model of the 17th century great earthquake off Hokkaido using tsunami deposit data. Earth Planet Sci Lett 433:133–138. https://doi.org/10.1016/j.epsl.2015.10.009

Iwagaki Y (1956) Hydrodynamical study on critical tractive force. Trans Jpn Soc Civil Eng 41:1–21. https://doi.org/10.2208/jscej1949.1956.41_1 (**In Japanese, with English abstract**)

Iwasaki T, Sato H, Shinohara M, Ishiyama T, Hashima A (2015) Fundamental structure model of island arcs and subducted plates in and around Japan. 2015 Fall Meeting American Geophysical Union, San Francisco, Dec 14–18, 2015.

Jaffe BE, Gelfenbaum G (2007) A simple model for calculating tsunami flow speed from tsunami deposits. Sediment Geol 200:347–361. https://doi.org/10.1016/j.sedgeo.2007.01.013

Jaffe B, Goto K, Sugawara D, Gelfenbaum G, La Selle S (2016) Uncertainty in tsunami sediment transport modeling. J Disaster Res 11:647–661. https://doi.org/10.20965/jdr.2016.p0647

Japan Society of Civil Engineers (2002) Tsunami assessment method for nuclear power plants in Japan. https://committees.jsce.or.jp/ceofnp/system/files/JSCE_Tsunami_060519.pdf. Accessed 9 Feb 2022

Kempf P, Moernaut J, Van Daele M, Vandoorne W, Pino M, Urrutia R, De Batist M (2017) Coastal lake sediments reveal 5500 years of tsunami history in south central Chile. Quat Sci Rev 161:99–116. https://doi.org/10.1016/j.quascirev.2017.02.018

Kotani M, Imamura F, Shuto N (1998) Tsunami run-up simulation and damage estimation by using GIS. Proc Coastal Eng, Jpn Soc Civil Eng 45:356–360. https://doi.org/10.2208/proce1989.45.356 (**In Japanese, translated title**)

Kusumoto S, Imai K, Gusuman AR, Satake K (2020) Reduction effect of tsunami sediment transport by a coastal forest: numerical simulation of the 2011 Tohoku tsunami on the Sendai Plain, Japan. Sediment Geol 407:105740. https://doi.org/10.1016/j.sedgeo.2020.105740

Lindquist KG, Engle K, Stahlke D, Price E (2004) Global topography and bathymetry grid improves research efforts. Eos 85:186. https://doi.org/10.1029/2004EO190003

Masaya R, Suppasri A, Yamashita K, Imamura F, Gouramanis C, Leelawat N (2020) Investigating beach erosion related with tsunami sediment

transport at Phra Thong Island, Thailand, caused by the 2004 Indian Ocean tsunami. Nat Hazards Earth Syst Sci 20:2823–2841. https://doi.org/10.5194/nhess-20-2823-2020

Masaya R, Yamashita K, Suppasri A, Imamura F (2021) A study on paleo-tsunami source estimation considering sediment source of tsunami deposits. J Jpn Soc Civil Eng Ser B2 77:I_289-I_294. https://doi.org/10.2208/kaigan.77.2_I_289 (**In Japanese, with English abstract**)

Minamidate K, Goto K, Kan H (2022) Numerical estimation of maximum possible sizes of paleo-earthquakes and tsunamis from storm-derived boulders. Earth Planet Sci Lett 579:117354. https://doi.org/10.1016/j.epsl.2021.117354

Minoura K, Nakaya S (1991) Traces of tsunami preserved in inter-tidal lacustrine and marsh deposits: some examples from northeast Japan. J Geol 99:265–287. https://doi.org/10.1086/629488

Mori N, Takahashi T, the 2011 Tohoku Earthquake Tsunami Joint Survey Group (2012) Nationwide post event survey and analysis of the 2011 Tohoku earthquake tsunami. Coastal Eng J 54:1250001. https://doi.org/10.1142/S0578563412500015

Murotani S, Satake K, Fujii Y (2013) Scaling relations of seismic moment, rupture area, average slip, and asperity size for M~9 subduction-zone earthquakes. Geophys Res Lett 40:5070–5074. https://doi.org/10.1002/grl.50976

Nakanishi R, Ashi J (2022) Sediment transport modeling based on geological data for Holocene coastal evolution: wave source estimation of sandy layers on the coast of Hidaka, Hokkaido, Japan. J Geophys Res Earth Surf 127:e2022JF006721. https://doi.org/10.1029/2022JF006721

Namegaya Y, Satake K (2014) Reexamination of the A.D. 869 Jogan earthquake size from tsunami deposit distribution, simulated flow depth, and velocity. Geophys Res Lett 41:2297–2303. https://doi.org/10.1002/2013GL058678

Naruse H, Abe T (2017) Inverse tsunami flow modeling, including nonequilibrium sediment transport, with application to deposits from the 2011 Tohoku-Oki tsunami. J Geophys Res Earth Surf 122:2159–2182. https://doi.org/10.1002/2017JF004226

Nettles M, Göran E, Howard CK (2011) Centroid-moment-tensor analysis of the 2011 off the Pacific coast of Tohoku Earthquake and its larger foreshocks and aftershocks. Earth Planets Space 63:519–523. https://doi.org/10.5047/eps.2011.06.009

Okada Y (1985) Surface deformation due to shear and tensile faults in a half-space. Bull Seismol Soc Am 75:1135–1154. https://doi.org/10.1785/BSSA0750041135

Putra PS, Nishimura Y, Nakamura Y, Yulianto E (2013) Sources and transportation modes of the 2011 Tohoku-Oki tsunami deposits on the central east Japan coast. Sediment Geol 294:282–293. https://doi.org/10.1016/j.sedgeo.2013.06.004

Richardson JF, Zaki WN (1954) Sedimentation and fluidisation: part I. Trans Inst Chem Eng 32:35–50

Rubey WW (1933) Settling velocity of gravel, sand, and silt particles. Am J Sci 25:325–338. https://doi.org/10.2475/ajs.s5-25.148.325

Satake K (1987) Inversion of tsunami waveforms for the estimation of a fault heterogeneity: method and numerical experiments. J Phys Earth 35:241–254. https://doi.org/10.4294/jpe1952.35.241

Satake K, Tanioka Y (1999) Sources of tsunami and tsunamigenic earthquakes in subduction zones. Pure Appl Geophys 154:467–483. https://doi.org/10.1007/s000240050240

Satake K, Namegaya Y, Yamaki S (2008) Numerical simulation of the AD 869 Jogan tsunami in Ishinomaki and Sendai plains. Annu Rep Act Fault Paleoearthq Res 8:71–89 (**In Japanese, with English abstract**)

Satake K, Fujii Y, Harada T, Namegaya Y (2013) Time and space distribution of coseismic slip of the 2011 Tohoku earthquake as inferred from tsunami waveform data. Bull Seismol Soc Am 103:1473–1492. https://doi.org/10.1785/0120120122

Sawai Y, Fujii Y, Fujiwara O, Kamataki T, Komatsubara J, Okamura Y, Satake K, Shishikura M (2008) Marine incursions of the past 1500 years and evidence of tsunamis at Suijin-numa, a coastal lake facing the Japan Trench. The Holocene 18:517–528. https://doi.org/10.1177/0959683608089206

Sawai Y, Namegaya Y, Okamura Y, Satake K, Shishikura M (2012) Challenges of anticipating the 2011 Tohoku earthquake and tsunami using coastal geology. Geophys Res Lett 39:L21309. https://doi.org/10.1029/2012GL053692

Sawai Y, Namegaya Y, Tamura T, Nakashima R, Tanigawa K (2015) Shorter intervals between great earthquakes near Sendai: Scour ponds and a sand layer attributable to A.D. 1454 overwash. Geophys Res Lett 42:4795–4800. https://doi.org/10.1002/2015GL064167

Shinozaki T, Goto K, Fujino S, Sugawara D, Chiba T (2015) Erosion of a paleo-tsunami record by the 2011 Tohoku-oki tsunami along the southern Sendai Plain. Mar Geol 369:127–136. https://doi.org/10.1016/j.margeo.2015.08.009

Skarlatoudis AA, Somerville PG, Thio HK (2016) Source-scaling relations of interface subduction earthquakes for strong ground motion and tsunami simulation. Bull Seismol Soc Am 106:1652–1662. https://doi.org/10.1785/0120150320

Smith WHF, Wessel P (1990) Gridding with continuous curvature splines in tension. Geophysics 55:293–305. https://doi.org/10.1190/1.1442837

Spiske M, Tang H, Bahlburg H (2020) Post-depositional alteration of onshore tsunami deposits: Implications for the reconstruction of past events. Earth-Sci Rev 202:103068. https://doi.org/10.1016/j.earscirev.2019.103068

Srinivasalu S, Thangadurai N, Switzer AD, Ram Mohan V, Ayyamperumal T (2007) Erosion and sedimentation in Kalpakkam (N Tamil Nadu, India) from the 26th December 2004 tsunami. Mar Geol 240:65–75. https://doi.org/10.1016/j.margeo.2007.02.003 (**In Japanese, with English abstract**)

Sugawara D (2019) On tsunami sediment transport modeling and uncertainties. Quat Res (Daiyonki-Kenkyu) 58:187–194. https://doi.org/10.4116/jaqua.58.187 (**In Japanese, with English abstract**)

Sugawara D (2021) Numerical modeling of tsunami: Advances and future challenges after the 2011 Tohoku earthquake and tsunami. Earth-Sci Rev 214:103498. https://doi.org/10.1016/j.earscirev.2020.103498

Sugawara D, Goto K, Jaffe B (2014a) Numerical models of tsunami sediment transport: current understanding and future directions. Mar Geol 352:295–320. https://doi.org/10.1016/j.margeo.2014.02.007

Sugawara D, Takahashi T, Imamura F (2014b) Sediment transport due to the 2011 Tohoku-oki tsunami at Sendai: results from numerical modeling. Mar Geol 358:18–37. https://doi.org/10.1016/j.margeo.2014.05.005

Sugawara D, Jaffe B, Goto K, Gelfenbaum G, La Selle S (2015) Exploring hybrid modeling of tsunami flow and deposit characteristics. In: Wang P, Rosati JD, Cheng J (eds) The proceedings of the coastal sediments. San Diego, May 11–15, 2015. https://doi.org/10.1142/9789814689977_0185

Sugawara D, Yu NT, Yen JY (2019) Estimating a tsunami source by sediment transport modeling: a primary attempt on a historical/1867 normal-faulting tsunami in northern Taiwan. J Geophys Res Earth Surf 124:1675–1700. https://doi.org/10.1029/2018JF004831

Suppasri A, Koshimura S, Imai K, Mas E, Gokon H, Muhari A, Imamura F (2012) Damege characteristics and field survey of the 2011 Great East Japan Tsunami in Miyagi Prefecture. Coastal Eng J 54:1250005. https://doi.org/10.1142/S0578563412500052

Szczuciński W (2012) The post-depositional changes of the onshore 2004 tsunami deposits on the Andaman Sea coast of Thailand. Nat Hazards 60:115–133. https://doi.org/10.1007/s11069-011-9956-8

Szczuciński W, Kokociński M, Rzeszewski M, Chagué-Goff C, Cachão M, Goto K, Sugawara D (2012) Sediment sources and sedimentation processes of 2011 Tohoku-oki tsunami deposits on the Sendai Plain, Japan: insights from diatoms, nannoliths and grain size distribution. Sediment Geol 282:40–56. https://doi.org/10.1016/j.sedgeo.2012.07.019

Takahashi T, Kurokawa T, Fujita M, Shimada H (2011) Hydraulic experiment on sediment transport due to tsunamis with various sand grain size. J Jpn Soc Civil Eng Ser B2 67:I_231–I_235. https://doi.org/10.2208/kaigan.67.I_231 (**In Japanese, with English abstract**)

Takahashi T, Shuto N, Imamura F, Asai D (2000) Modeling sediment transport due to tsunamis with exchange rate between bed load layer and suspended load layer. In: Edge BL (ed) Proceedings of the 27th international conference on coastal engineering. Sydney, July 16–21, 2000. https://doi.org/10.1061/40549(276)117

Takashimizu Y, Urabe A, Suzuki K, Sato Y (2012) Deposition by the 2011 Tohoku-oki tsunami on coastal lowland controlled by beach ridges near Sendai, Japan. Sediment Geol 282:124–141. https://doi.org/10.1016/j.sedgeo.2012.07.004

Tang H, Weiss R (2015) A model for tsunami flow inversion from deposits (TSUFLIND). Mar Geol 370:55–62. https://doi.org/10.1016/j.margeo.2015.10.011

Tanioka Y, Satake K (1996) Tsunami generation by horizontal displacement of ocean bottom. Geophys Res Lett 23:861–864. https://doi.org/10.1029/96GL00736

van Rijn LC (2007) Unified view of sediment transport by currents and waves. II: suspended transport. J Hydraul Eng 133:668–689. https://doi.org/10.1061/(ASCE)0733-9429(2007)133:6(668)

Wessel P, Luis JF, Uieda L, Scharroo R, Wobbe F, Smith WHF, Tian D (2019) The Generic Mapping Tools version 6. Geochem Geophys Geosyst 20:5556–5564. https://doi.org/10.1029/2019GC008515

Yamashita K, Sugawara D, Takahashi T, Imamura F, Saito Y, Imato Y, Kai T, Uehara H, Kato T, Nakata K, Saka R, Nishikawa A (2016) Numerical simulations of large-scale sediment transport caused by the 2011 Tohoku earthquake tsunami in Hirota Bay, southern Sanriku Coast. Coastal Eng J 58:16400015. https://doi.org/10.1142/S0578563416400155

Yamashita K, Sugawara D, Arikawa T, Shigihara Y, Takahashi T, Imamura F (2018) Improvement of tsunami-induced sediment transport model by considering saturated concentration in suspension with strong unsteady flows. J Jpn Soc Civil Eng Ser B2 74:I_325-I_330. https://doi.org/10.2208/kaigan.74.I_325 (**In Japanese, with English abstract**)

Yamazaki Y, Cheung KF, Lay T (2018) A self-consistent fault slip model for the 2011 Tohoku earthquake and tsunami. J Geophys Res Solid Earth 123:1435–1458. https://doi.org/10.1002/2017JB014749

Yoshikawa S, Kanamatsu T, Goto K, Sakamoto I, Yagi M, Fujimaki M, Imura R, Nemoto K, Sakaguchi H (2015) Evidence for erosion and deposition by the 2011 Tohoku-oki tsunami on the nearshore shelf of Sendai Bay, Japan. Geo-Mar Lett 35:315–328. https://doi.org/10.1007/s00367-015-0409-3

Yoshikawa S, Goto K, Sugawara D, Kanamatsu T, Sakaguchi H (2017) Nearshore erosion and offshore-directed sediment transport by Tohoku-oki tsunami off southern part of the Sendai Plain. J Jpn Soc Civil Eng Ser B2 73:I_823-I_828. https://doi.org/10.2208/kaigan.73.I_823 (**In Japanese, with English abstract**)

Yoshikawa S, Sugawara D, Goto K, Sato A, Kanamatsu T, Sakaguchi H (2018) Numerical simulation for understanding of the offshore- directed sediment transport by 2011 Tohoku-oki tsunami at southern part of the Sendai Bay. J Jpn Soc Civil Eng Ser B2 74:I_337-I_342. https://doi.org/10.2208/kaigan.74.I_337 (**In Japanese, with English abstract**)

Publisher's Note